

Article

Finite Element Analysis and Electrohydrodynamic Multiphysics Modeling of a Corona-Streamer Discharge in a Two-Phase Flow Medium

Myung-Ki Baek ¹ and Ho-Young Lee ^{2,*} 

¹ Numerical Analysis Technology Support Department, Korea Electrotechnology Research Institute, Changwon 51543, Republic of Korea; mkbaek@keri.re.kr

² Division of Smart Convergence Engineering, Changshin University, Changwon 51352, Republic of Korea

* Correspondence: hylee@cs.ac.kr; Tel.: +82-55-250-1302

Abstract: This study proposes an electrohydrodynamic multiphysics modeling and finite element analysis technique to accurately simulate corona-streamer discharges in a two-phase flow medium. The discharge phenomenon is modeled as a multiphysics system, coupling the Poisson equation for the electric field with a charge dynamics model based on fluid methods and a thermofluid field for temperature effects. To optimize the numerical simulation, the tip-flat plate electrode model was simplified to two-dimensional axisymmetry, and an unordered lattice network was used to reduce computational time while maintaining high resolution in the region of interest. A high DC voltage was applied to the model to generate a local non-uniform electric field exceeding 10 MV/m, allowing the numerical simulations of ionization, recombination, and charge attachment in the streamer channel. The numerical results were compared with voltage and current measurements from full-scale experiments under identical geometry and initial conditions to verify the effectiveness of the proposed method. The results of this study enhance the understanding of the multiphysical mechanisms behind electrical discharge phenomena and can enable the prediction of insulation failure through simple simulations, eliminating insulation experiments on devices.



Academic Editor: Claus Leth Bak

Received: 20 November 2024

Revised: 22 January 2025

Accepted: 30 January 2025

Published: 1 February 2025

Citation: Baek, M.-K.; Lee, H.-Y. Finite Element Analysis and Electrohydrodynamic Multiphysics Modeling of a Corona-Streamer Discharge in a Two-Phase Flow Medium. *Energies* **2025**, *18*, 680. <https://doi.org/10.3390/en18030680>

Copyright: © 2025 by the authors. Licensee MDPI, Basel, Switzerland. This article is an open access article distributed under the terms and conditions of the Creative Commons Attribution (CC BY) license (<https://creativecommons.org/licenses/by/4.0/>).

Keywords: electrohydrodynamics; multiphysics modeling; finite element analysis; corona streamer; electric discharge

1. Introduction

With rapid industrialization and the development of an advanced digital society, electricity demand has increased significantly. In power systems operating at high voltages and currents, efforts are being made to address various insulation issues, such as preventing the deterioration of insulating fluids and improving cooling performance, to enhance the efficiency of power devices [1–3]. Particularly, space charge accumulation inside insulating fluids can lead to serious accidents [4,5]. Therefore, various electrical discharge studies including gas, fluid, and solid dielectric discharges have been conducted to prevent electrical stress while designing devices [6–10].

Until now, research on insulating fluids in the field of power equipment has relied on experiments conducted outside of devices, which not only causes significant economic losses in the design and operation of test devices but also makes it difficult to analyze the physical phenomena occurring inside the devices. The multiphysics numerical simulation method proposed in this study is a new, physics-based simulation technique that can

overcome these experimental limitations. Figure 1 shows a schematic of the numerically modeled multiphysics system interactions in an insulating fluid. Multiphysics numerical simulations are conducted by combining electric, charge kinetic, temperature, and heat flow fields into a continuum system, along with multiphysics variables that reflect each physical phenomenon. Bubbles that form simultaneously with streamer initiation directly impact insulation breakdown. Therefore, a two-phase flow must be considered for simulation. Finite element analysis of the brain impulse response to a two-phase flow includes the Poisson equation for the electric field and charge continuity equations for electrons, cations, and anions, with field and thermoelectric emission effects as boundary conditions. The gas ionization phenomena are mathematically modeled using Townsend's theory, while the fluid ionization phenomena are combined into a two-phase flow using the Zener ionization model. Numerical instabilities caused by the hydrodynamic treatment of charges in multiphysics models are mitigated by introducing dimensionless and artificial diffusion terms [11,12]. These multiphysics models are validated by a comparative analysis of theoretical and numerical solutions, which includes terminal current calculations using the energy method, applied to an electrohydrodynamic model [13]. The required electrodes are designed according to the standard specifications of IEC 60897 [14], and a reliable numerical analysis method is presented by applying it to a two-dimensional axisymmetric simplified model, comparing the results with experimental data.

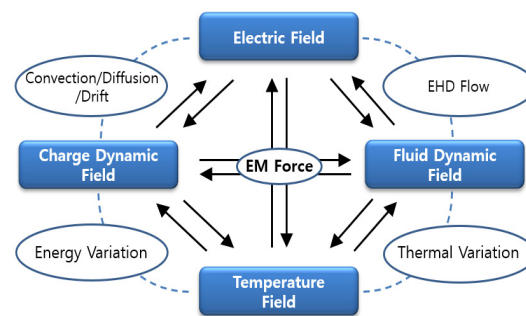


Figure 1. Schematic of multiphysics for space charge transport in a dielectric liquid.

In this paper, the positive and negative polarity discharge mechanisms were explained using numerical analysis techniques applicable to air- and oil-based two-phase electrical discharge problems. To calculate the space charge propagation, the governing equations were selected and combined, including the charge continuity equation for hydrodynamic drift–diffusion, the Poisson equation for electric fields, and the heat transfer equation for temperature. Numerical analysis was performed using a two-dimensional axisymmetric tip-plate model, and the initiation and propagation processes of pulsed currents formed by both positive and negative discharges as well as negative corona-streamer discharges were quantitatively investigated. Since modeling of such electrical discharge dynamics involves several fields, including electrodynamics, fluid dynamics, and thermodynamics, a finite element-based COMSOL MULTIPHYSICS 3.5a was used to perform a flexible analysis.

2. Characteristics of Electric Corona-Streamer Discharges

2.1. Positive Polarity Corona-Streamer Discharge

In an electrochemical discharge model comprising a needle and flat plate electrode, the electrostatic corona discharge phenomenon is caused by a non-uniform electric field concentrated around the anode-connected settling electrode. This phenomenon starts as a dark current around the settling electrode and progresses to a glowing corona, which then evolves to a streamer corona as the voltage applied between the electrodes increases. When the streamer reaches the flat electrode, the discharge path is interrupted, resulting

in a spark discharge. Figure 2 illustrates the growth of a bipolar corona discharge as a function of applied voltage [15].

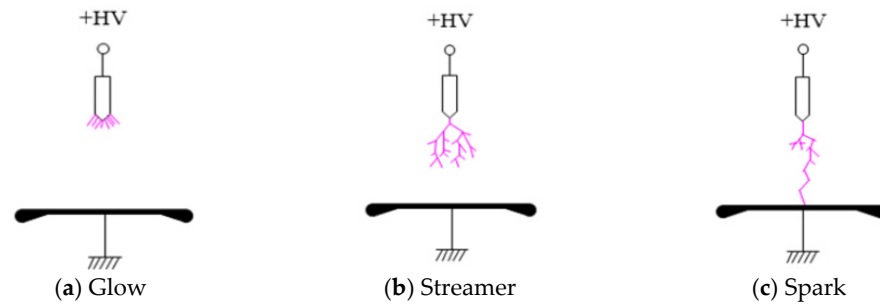


Figure 2. Shape of positive corona-streamer discharge.

2.2. Negative Polarity Corona-Streamer Discharge

The negative corona discharge is generated by the potential difference between the cathodically connected needle electrode and the flat plate electrode. Unlike the positive corona, the negative corona discharge occurs immediately following the Trichel pulse corona. The Trichel pulse is caused by secondary electron emission from the cathode. When a Trichel pulse is generated, a red glow near the settling electrode develops outward from the cathode surface, pulsating rapidly and continuously throughout the circuit. Figure 3 shows the development of the negative corona discharge as the voltage increases [16,17].

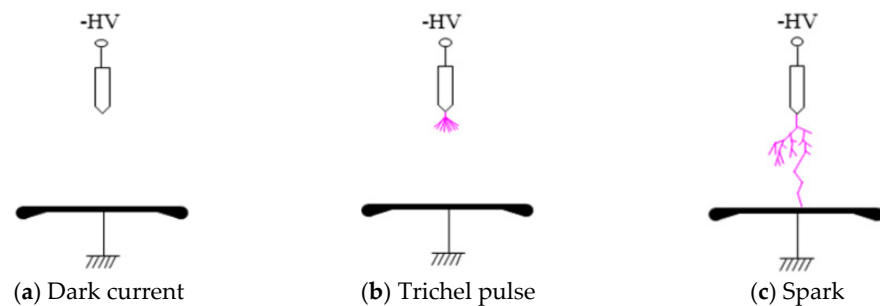


Figure 3. Shape of negative corona-streamer discharge.

3. Electrohydrodynamic Analysis Model

3.1. Governing Equations

The electrohydrodynamic analysis model comprises the Poisson equation for the electric field, accounting for the permittivity and space charge of the medium in the computational domain; the charge continuity equation, which considers the molecular ionization of each charge, ionic dissociation, recombination between charges, and charge attachment; and the heat diffusion equation for temperature.

$$-\nabla \cdot (\epsilon \nabla V) = \rho_+ + \rho_- + \rho_e \quad (1)$$

$$\frac{\partial \rho_+}{\partial t} + \nabla \cdot (\rho_+ \mu_+ \vec{E}) = \left[G_I(\vec{E}) + \frac{\rho_+ \rho_e R_{+e}}{e} + \frac{\rho_+ \rho_- R_{+-}}{e} \right] (1 - H(W - W_0)) + G_{I \text{ gas}}(\vec{E}) H(W - W_0) \quad (2)$$

$$\frac{\partial \rho_e}{\partial t} - \nabla \cdot (\rho_e \mu_e \vec{E}) = \left[-G_I(\vec{E}) - \frac{\rho_+ \rho_e R_{+e}}{e} - \frac{\rho_e}{\tau_a} \right] (1 - H(W - W_0)) - G_{I \text{ gas}}(\vec{E}) H(W - W_0) \quad (3)$$

$$\frac{\partial \rho_-}{\partial t} - \nabla \cdot (\rho_- \mu_- \vec{E}) = \left[\frac{\rho_e}{\tau_a} - \frac{\rho_+ \rho_- R_{+-}}{e} \right] (1 - H(W - W_0)) \quad (4)$$

$$\frac{\partial T}{\partial t} + \vec{u} \cdot \nabla T = \rho_l c_v \left(k_T \nabla^2 T + \vec{E} \cdot \vec{J} \right) \quad (5)$$

where ε is the permittivity of the medium, V is the electrical potential, ρ_+ , ρ_- and ρ_e are the cation density, anion density, and electron charge density. μ_+ , μ_- , and μ_e are the mobilities of cation, anion, and electron, respectively. \vec{E} is the electric field vector. Current density considers the convection and diffusion of charges. Here, G_I denotes the charge generation term, which includes the ionization of molecules for cations and electrons, and the dissociation of ions for anions and cations. R_{+e} and R_{+-} are the recombination rate between each charge, and τ_a represents the attachment of an electron to a neutral ion to create an anion. T is the temperature of the liquid in Kelvin. Further, \vec{u} , ρ_l , c_v , and k_T represent the velocity, mass density, specific heat, and thermal diffusivity of the liquid, respectively. $\vec{E} \cdot \vec{J}$ denotes the electric power loss that takes place in the fluid as a result of the motion of free charges under the influence of the local electric field [11,12]. In this model, the term $H(W - W_0)$ represents the smoothed Heavyside function. This function is used to switch between liquid and gas phase physics by comparing the dissipated energy density W of the liquid with the threshold value W_0 . Specifically, if W is lower than W_0 , $H(W - W_0)$ becomes 0, and the liquid phase model is applied. If W exceeds W_0 , $H(W - W_0)$ becomes 1, and the gas phase model is activated. This allows the model to modify the charge carrier mobility according to the phase state of the fluid. $G_{I\ gas}$ also refers to the term gas phase-free charge source, which is caused by impact ionization within the streamer channel.

3.2. Ionization in the Gas Phase

Electrons in the gas space move freely until they collide with a neutron. Electrons accelerated by the electric field to high energies ionize new neutrons, generating more free electrons exponentially. According to Townsend's theory, electrons accelerated by the electric field ionize neutrons in space, leading to a rapid increase in current. Therefore, the gas ionization source term of the two-phase flow can be mathematically modeled by introducing Townsend's theory, which is expressed as follows [18]:

$$G_{I\ gas}(\vec{E}) = -\alpha_T \rho_e \mu_{eGP} |\vec{E}| \quad (6)$$

where α_T is the Townsend ionization first-order coefficient, which is the number of charge collisions per unit distance in the gas phase, μ_{eGP} is the free electron mobility in the gas phase, and $|\vec{E}|$ is the magnitude of the electric field. The gas ionization source term in the two-phase flow causes a potential drop in the streamer channel.

3.3. Ionization in the Dielectric Fluid Phase

When no external forces act on a dielectric fluid, the atoms remain stable and share electrons. When neutral molecules are exposed to a strong electric field, they lose their outermost electrons and become charged, forming cations and free electrons. The ionizing source term of the charge in response to a high field is assumed to follow a charge density ratio based on the electron tunneling behavior of the dielectric. When applied to the Zener ionization model, the term can be expressed as follows [19,20]:

$$G_{I\ gas}(\vec{E}) = \frac{e^2 n_0 a |\vec{E}|}{h} \exp\left(-\frac{m^* a \pi \Delta^2}{eh^2 |\vec{E}|}\right) \quad (7)$$

where e is the elementary charge, n_0 is the density of molecules that can be ionized, a is the molecular separation constant, h is the Planck's constant, m^* is the effective mass of the insulating fluid, and Δ is the ionization energy of a molecule. Molecular electrolysis

involves several chemical reactions; however, this study is limited to the mechanism by which heavy components react under the influence of an electric field and are separated into cations and electrons, generating two free charges.

4. Experimental and Multiphysics Analysis of Corona-Streamer Discharges

4.1. Experimental Results

Figure 4a shows a schematic of the test model comprising a tip needle electrode and a flat-cell plate electrode. The experimental apparatus consisted of a discharger module with stainless steel electrodes for current verification, a high-voltage DC power supply, and high-voltage and current measurement devices. The experimental chamber comprised transparent acrylic to facilitate the observation of the internal phenomena. A micrometer head was used for precise electrode spacing adjustment, which could be adjusted for micro-displacements. A DC power supply of 30 kV was used, along with a 10 mA high-voltage transformer and a full-wave rectifier circuit using high-voltage diodes. Voltage and current were measured using a digital multimeter (Fluke 15B+, Fluke Corporation, Everett, WA, USA), an oscilloscope (KEYSIGHT DSOX 1202A, Keysight Technologies, Santa Rosa, CA, USA), a high-voltage probe (Tektronix P6015A, Tektronix Inc., Beaverton, OR, USA), an ultra-high-speed camera (Chronos 1.4, Kron Technologies Inc., Burnaby, BC, Canada), a set of protective resistors, and measuring resistors ($R_c = 1 \text{ k}\Omega$, $R_{s0} = 10 \text{ M}\Omega$). Figure 4b shows the flat-cell plate electrode used for current measurement. The measured current presented the real-time current for each channel from channels 1 to 8. Figures 5 and 6 show the experimental results for positive and negative polarity DC corona discharges. The positive polarity corona streamer originated from the tip of the needle electrode and propagated in a straight line from the high-field to the low-field region. Contrarily, the negative polarity streamer propagated radially, centered on the high-field region, and generated a Trichel pulse corona. With an electrode spacing of 2 mm in the positive polarity DC corona discharge, stepwise phenomena were observed as the voltage gradually increased. The voltage thresholds for different streamer types were clearly distinguished: 4.2, 4.23, and 4.37 kV for the single-channel streamer, multi-channel streamer, and insulation breakdown spark, respectively. In this study, corona discharge was measured to have different characteristics when subjected to positive and negative polarities. When the line is positively charged, the corona of the thin line uniformly covers the surface of the line with a bluish discharge, but when the line is negatively charged, it gradually turns red along the line, and the number of dots increases with the current. When the tip was non-polar in the flatbed electrode structure, it was measured that the triplet pulses appeared in a fairly regular repetition. Generally, the frequency of the triode pulse increases with voltage and is known by the curvature radius of the negative electrode, the distance between the electrodes, and the pressure. The results measured in this study indicate that the occurrence of triplet pulses is not significantly related to the distance between the electrodes. If the voltage is further increased, the Trichel pulse generation is converted to a constant glow discharge, and if the voltage is further increased, the glow discharge continues until the breakdown of the insulation.

Negative polarity required a higher applied voltage than positive polarity because the Trichel pulse corona was formed under conditions of secondary electron emission. The process required a sufficient element network and space to support the multiphysics interactions among cations, anions, and electron charges associated with the space charge.

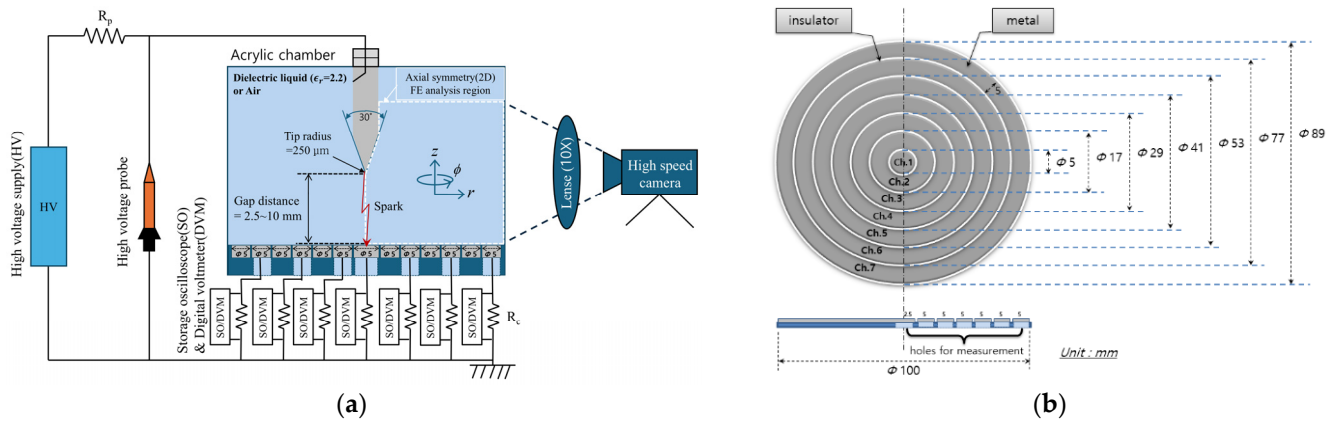


Figure 4. Schematic of the corona-stremer surface discharge analysis model. (a) Analytical and experimental model. (b) Flat-cell plate electrodes for measuring current.

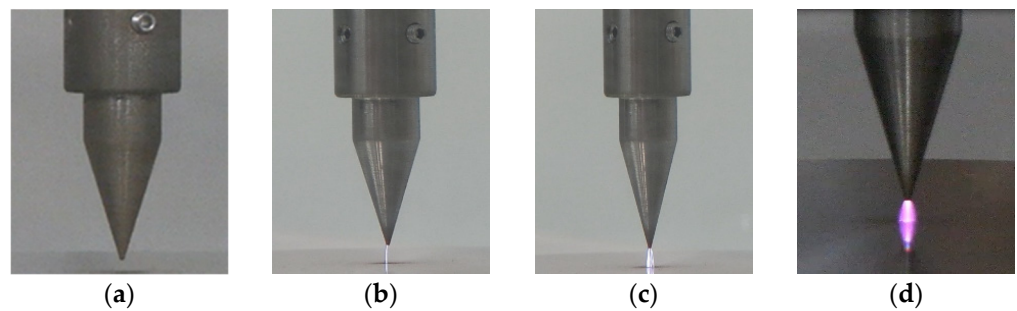


Figure 5. Experimental results of a positive polarity corona-stremer discharge (electrode gap = 2 mm). (a) Dark current corona (less than 4.2 kV), (b) single-channel streamer ($V = 4.2$ kV), (c) multi-channel streamer ($V = 4.23$ kV), and (d) spark (breakdown, $V = 4.37$ kV).

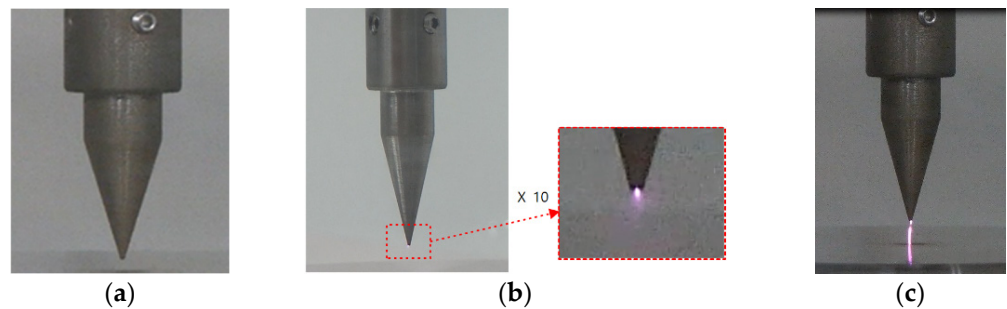


Figure 6. Experimental results of a negative polarity corona-stremer discharge (electrode gap = 5 mm). (a) Dark current corona (less than 6.9 kV), (b) Trichel pulse corona ($V = 6.9$ kV), and (c) spark (breakdown, $V = 7.17$ kV).

As shown in Figure 7a, the Trichel pulse corona was measured on a tip electrode with a radius of $100 \mu\text{m}$, placed 5 mm from the flat-cell plate electrode. When a negative dipolar DC voltage of 6.9 kV was applied, the current ranged from 10 to $100 \mu\text{A}$, with a frequency of 400 kHz. Figure 7b shows the current density at each cell electrode, measured at the flat-cell plate electrode after the Trichel pulse corona was initiated. The highest current density was observed in the channel perpendicular to the needle electrode, and it decreased with distance from the center. In Figure 7a, the growth time of the Trichel pulse corona (marked as A) was 97.5 ns, while the decay time (marked as B) was measured at 20 ns. The growth time of the Trichel pulse required approximately 4.9 times more time than the decay time.

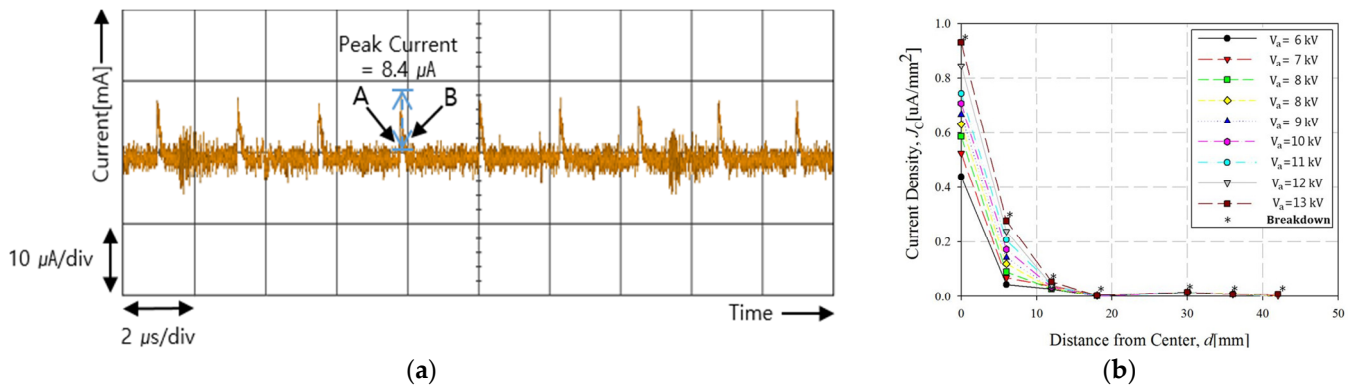


Figure 7. Experimental results of a negative polarity corona-streamer discharge. (a) Trichel pulse current measured from experiments. (b) Distribution of current density utilizing a flat-cell plate electrode.

4.2. Numerical Results

In this study, electrode geometry was represented according to the IEC 60897 standard specification model and modeled as a left–right symmetrical structure along the z -axis of the Cartesian coordinate system. We considered a two-dimensional axisymmetric spatial dimension [14]. For multiphysics finite element analyses such as electrical discharges, using a very small grid can significantly increase analysis time, particularly if the grid is generated to produce highly accurate results. Therefore, a local grid generation technique was used to divide the region of interest into substructures and vary the information for specific faces, lines, and nodes. Additionally, by performing a total of 10 analytical steps with a time interval of $0.1 \mu\text{s}$, system resource shortage was prevented, and an efficient analysis was achieved. The insulation in the simulation model was assumed to be pure transformer oil, and corona streamers were generated when a strong external electric field was applied. An uneven field was created at the precipitating electrode of the electrode model, leading to the formation of a streamer channel. When the field strength exceeded $1\text{--}100 \text{ kV/m}$, free electrons were released from the electrode and collided with neutral particles in the insulating fluid, resulting in phenomena such as ionization, dissociation, recombination, and electron attachment.

Figure 8a shows the simulation results of the streamer and the propagation process of a monopolar corona, where the space charge distribution propagated from the needle to the flat plate electrode over time. When a DC voltage exceeding 3 kV was applied to the tip electrode of the simulation model, a local electric field exceeding $10\text{--}100 \text{ MV/m}$ was formed. Further, the space charge began to diffuse and propagate. When a negative DC voltage was applied and the electric field around the needle exceeded 10 MV/m , Trichel pulse corona was generated, as shown in Figure 8b. The space charge originated at the needle and propagated radially up to approximately 200 ns under the influence of secondary electron emission. When the charge reached insulation breakdown, it released thermal energy and propagated to the flat plate.

Figure 9a shows the measured breakdown voltages of air and oil as the medium in the electric discharge model of the flat-tip plate model. It can be seen that the measured breakdown voltage of oil discharge is approximately five times that of air discharge. Figure 9b shows the electric field distribution dynamics along the electrode axis between the flat-tip plate electrodes predicted by the two-phase model at $0.1 \mu\text{s}$ intervals between $t = 0.3 \mu\text{s}$ and $t = 1.0 \mu\text{s}$. The electric field distribution at $t = 0.3 \mu\text{s}$ represents the Laplacian electric field distribution generated by the flat-tip plate electrode geometry. A very interesting and important feature of the electric field dynamics generated by the two-phase model is the fact that the peak of the electric field distribution does not occur at the tip of the needle electrode, as in the Laplacian field distribution, but at a point in the oil gap between the

needle and the spherical electrode, and that the position of the peak of the electric field shifts with time from the needle electrode to the plate electrode. At the beginning of the simulation, a high-field region was formed at the settling pole along the Laplacian field distribution. After approximately $0.4 \mu\text{s}$, a field wave propagated with a field strength of $5.5 \times 10^8 \text{ V/m}$. A sharp potential change occurred at the peak of the field wave, attributed to the two-phase flow medium. Figure 9c shows the distribution of cations and anions as a function of time during streamer propagation from the needle electrode ($x = 0$) to the flat plate electrode. The cations in the streamer channel were relatively more abundant than the anions, attributing to charge generation due to the ionization of molecules. Figure 9d shows the propagation of the injected electrons in space by field and thermal electron emissions. Compared with the results shown in Figure 2, the space charge was concentrated in the space where the peak of the field wave was formed. Free electrons migrated to the needle electrode at a faster rate than the ions. The ionization of molecules by the electric field was considered to be the main source of free charge generation. The charges separated from the stable neutral species moved along the electric field in the dielectric and formed space charges owing to the different mobilities of electrons and ions.

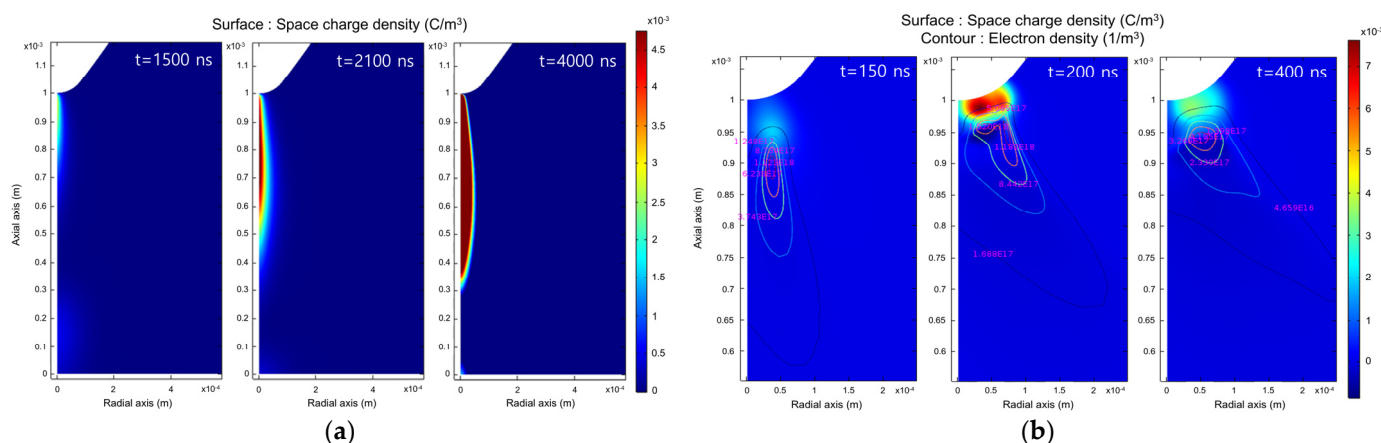


Figure 8. Results from the multiphysics analysis of corona-streamer discharges. (a) Creating streamers and propagating space charges. (b) Trichel pulse generation and space charge diffusion. The scientific notation ‘8E3’ in the figure means ‘ 8×10^3 ’.

Corona streamers in insulating fluids, where a two-phase flow medium was considered, occurred at the precipitating electrode, where a local uneven electric field was formed, driving the streamer channel toward the flat plate electrode. A discontinuous field of approximately 10 MV/m was distributed within the two-phase flow medium inside the streamer channel and was believed to be responsible for the bubbles that appeared around the streamer. The potential drop in the insulating fluid occurred at the tail of the electric field wave, and the validity of the proposed numerical method was verified by comparing the potential drop per unit length with the experimental measurements.

Table 1 lists the simulation results of the measurements in the two-phase flow medium. Compared with the experimental values, the maximum current value predicted by the multiphysics simulation was on average 13.6% less. In addition, the average velocity of the streamer measured in the experiment was 1.5 km/s , which was 2.4 to 4.4 times faster in the numerical simulation results. To improve the accuracy of the simulation predictions in the future, further research is required to consider the roughness characteristics of the electrode surface and variations in the thermal properties of the medium.

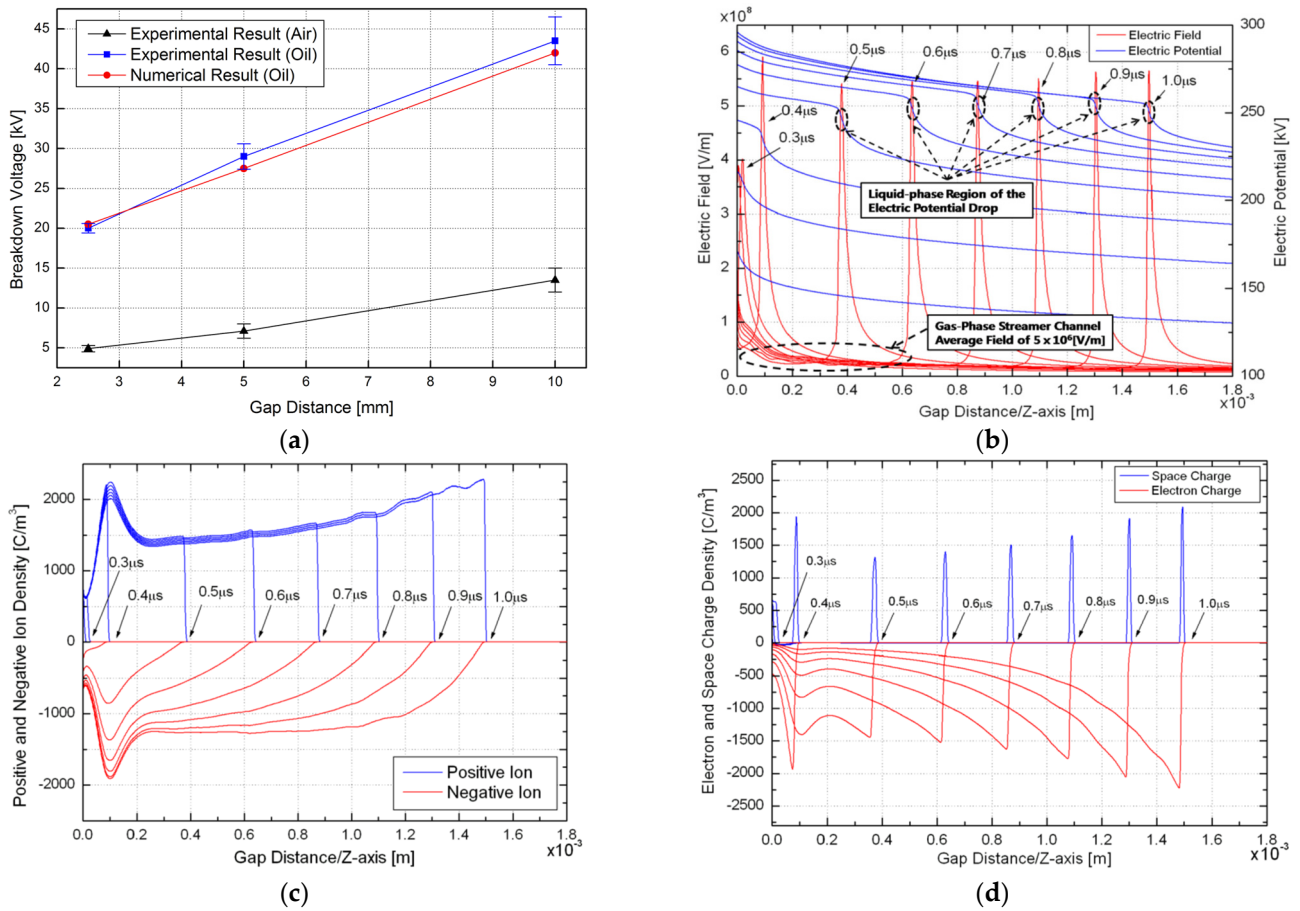


Figure 9. Analytical results of a positive polarity corona streamer in a two-phase flow medium. (a) Predictions and experimental results of breakdown voltage for flat-tip electrodes with gaps of 2.5 mm, 5 mm, and 10 mm. (b) Time dynamics of the electric field distribution along the tip-flat plate electrode axis predicted by a two-phase ionization model by applying positive voltage excitation to the needle electrode. (c) Distribution of the positive and negative ion density along the flat-tip plate electrode axis at 0.1 μ s intervals from $t = 0.3$ to 1.0 μ s given by the solution of the two-phase model. (d) Distribution of the electron and space charge density along the flat-tip plate electrode axis at 0.1 μ s intervals from $t = 0.3$ to 1.0 μ s given by the solution of the two-phase model.

Table 1. Experimental and numerical results in a two-phase flow medium.

Gap Distance (mm)	Experiment		Simulation	
	Breakdown Voltage	Peak Current (μ A)	Streamer Velocity (km/s)	Peak Current (μ A)
2.5	19.7 kV \pm 2.5%	4.7	6.7	3.92
5.0	27.0 kV \pm 5.0%	4.4	4.7	3.69
10.0	43.5 kV \pm 8.0%	4.0	3.7	3.39

5. Conclusions

In this study, a multiphysics modeling methodology is presented for the DC high field-constrained finite element analysis of a corona streamer with a local inequality field exceeding 10–100 MV/m at the tip electrode, considering the ionization, dissociation, attachment, and recombination of charges in the streamer discharge channel and secondary electron emission conditions. For the electrohydrodynamic approach of a two-phase flowing medium, the Poisson equation for the electric field; the charge continuity equation for electrons, cations, and anions; and the thermofluid equation for temperature are formulated as governing equations, and the effects of field emission and thermoelectric emission

are imposed as boundary conditions. In addition, the Townsend theory is adopted for the gas ionization phenomenon, and the Zener ionization model for the fluid ionization phenomenon is combined into a two-phase flow multiphysics system through mathematical modeling. A needle electrode is designed according to the standard specifications of IEC 60897, and a reliable numerical simulation method was proposed by applying it to a two-dimensional axisymmetric simplified model and comparing it with the experimental results. The experimental results of this study confirmed that corona discharge and triode pulses vary depending on the polarity of the electrode. In particular, the results showed that negative electrical discharge is converted from triaxial pulse to glow discharge, which eventually leads to insulation breakdown. The simulation results show that the electric field changes over time in both phase fluid media, and the maximum current is 13.6% lower and the streamer speed is 2.4 to 4.4 times faster compared to the experiment, confirming the need for research to improve the accuracy of future simulations.

The results of this study will enable the investigation of the mechanism of the electrical discharge phenomenon of corona streamers using multiphysics analysis and will be applied to the design and development of power equipment using insulating materials in the future.

Author Contributions: Data curation, formal analysis, and investigation, M.-K.B.; methodology, supervision, writing—original draft, writing—review and editing, H.-Y.L. All authors have read and agreed to the published version of the manuscript.

Funding: This research received no external funding.

Data Availability Statement: The original contributions presented in this study are included in the article. Further inquiries can be directed to the corresponding author.

Acknowledgments: This results was supported by “Regional Innovation Strategy (RIS)” through the National Research Foundation of Korea(NRF) funded by the Ministry of Education (MOE) (2021RIS-003).

Conflicts of Interest: The authors declare no conflicts of interest.

References

1. Nijdam, S.; Teunissen, J.; Ebert, U. The physics of streamer discharge phenomena. *Plasma Sources Sci. Technol.* **2020**, *29*, 103001. [[CrossRef](#)]
2. Ravindra, A.; Wolfgang, M. *High Voltage and Electrical Insulation Engineering*; John Wiley & Sons: Hoboken, NJ, USA, 2022.
3. Stone, G.C.; Cavallini, A.; Behrmann, G.; Serafino, C.A. *Practical Partial Discharge Measurement on Electrical Equipment*; John Wiley & Sons: Hoboken, NJ, USA, 2023.
4. Montanari, G.C.; Seri, P.; Bononi, S.F.; Albertini, M. Partial discharge behavior and accelerated aging upon repetitive DC cable energization and voltage supply polarity inversion. *IEEE Trans. Power Deliv.* **2020**, *36*, 578–586. [[CrossRef](#)]
5. Chen, G.; Zhao, J.; Li, S.; Zhong, L. Origin of thickness dependent DC electrical breakdown in dielectrics. *Appl. Phys. Lett.* **2012**, *100*, 222904. [[CrossRef](#)]
6. Min, D.; Wang, W.; Li, S. Numerical analysis of space charge accumulation and conduction properties in LDPE nanodielectrics. *IEEE Trans. Dielect. Electr. Insul.* **2015**, *22*, 1483–1491. [[CrossRef](#)]
7. Zhou, Y.; Wang, Y.; Li, G.; Wang, N.; Liu, Y.; Li, B.; Li, P.; Cheng, H. Space charge phenomena in oil-paper insulation materials under high voltage direct current. *J. Electrostat.* **2009**, *67*, 417–421. [[CrossRef](#)]
8. Cho, Y.S.; Hong, T.Y.; Youn, Y.W.; Sun, J.H.; Lee, S.H. Study on the correlation between partial discharge energy and SF₆ decomposition gas generation. *Energies* **2020**, *13*, 4655. [[CrossRef](#)]
9. Wang, W.; Yan, X.; Li, S.; Zhang, L.; Ouyang, J.; Ni, X. Failure of submarine cables used in high-voltage power transmission: Characteristics, mechanisms, key issues and prospects. *IET Gener. Transm. Distrib.* **2021**, *15*, 1387–1402. [[CrossRef](#)]
10. Kim, M.; Kim, S.H.; Lee, S.H. Finite element analysis of the breakdown prediction for LDPE stressed by various ramp rates of DC voltage based on molecular displacement model. *Energies* **2020**, *13*, 1320. [[CrossRef](#)]
11. Lee, H.Y.; Kang, I.M.; Lee, S.H. Fully coupled finite element analysis for surface discharge on solid insulation in dielectric liquid with experimental validation. *IEEE Trans. Magn.* **2016**, *52*, 1–4. [[CrossRef](#)]

12. Kang, H.M.; Park, D.G.; Han, S.B.; Hwang, D.H.; Lee, H.Y. Electro-hydrodynamic multiphysics analysis of surface discharge in corona-streamer. *Proc. KIEE Conf.* **2023**, *52*, 1625–1626.
13. Lee, H.Y.; Jung, J.S.; Kim, H.K.; Park, I.H.; Lee, S.H. Numerical and experimental validation of discharge current with generalized energy method and integral Ohm's law in transformer oil. *IEEE Trans. Magn.* **2014**, *50*, 257–260. [[CrossRef](#)]
14. IEC 60897; Methods for the Determination of the Lightning Impulse Breakdown Voltage of Insulating Liquids. International Electrotechnical Commission: London, UK, 1987.
15. Chang, J.S.; Lawless, P.A.; Yamamoto, T. Corona discharge processes. *IEEE Trans. Plasma Sci.* **1991**, *19*, 1152–1166. [[CrossRef](#)]
16. Van Brunt, R.J. Stochastic properties of partial discharge phenomena. *IEEE Trans. Electr. Insul.* **1991**, *26*, 902–948. [[CrossRef](#)]
17. Sattari, P.; Gallo, C.F.; Castle, G.S.P.; Adamiak, K. Trichel Pulse Characteristics—Negative Corona Discharge in air. *J. Phys. D Appl. Phys.* **2011**, *44*, 155502. [[CrossRef](#)]
18. O'Sullivan, F.; Hwang, J.G.; Zahn, M.; Hjortstam, O.; Pettersson, L.; Liu, R.; Biller, P. A model for the initiation and propagation of positive streamers in transformer oil. In Proceedings of the Conference Record of the 2008 IEEE International Symposium on Electrical Insulation, Vancouver, BC, Canada, 9–12 June 2008; pp. 210–214. [[CrossRef](#)]
19. Zener, C. A theory of the electrical breakdown of solid dielectrics. *Proc. R. Soc. Lond. A* **1934**, *145*, 523–529.
20. Devins, J.C.; Rzad, S.J.; Schwabe, R.J. Breakdown and Prebreakdown phenomena in liquids. *J. Appl. Phys.* **1981**, *52*, 4531–4545. [[CrossRef](#)]

Disclaimer/Publisher's Note: The statements, opinions and data contained in all publications are solely those of the individual author(s) and contributor(s) and not of MDPI and/or the editor(s). MDPI and/or the editor(s) disclaim responsibility for any injury to people or property resulting from any ideas, methods, instructions or products referred to in the content.